Journal of Catalysis 366 (2018) 16–27

Contents lists available at ScienceDirect

Journal of Catalysis

journal homepage: www.elsevier.com/locate/jcat

Gas phase glycerol dehydration over H-ZSM-5 zeolite modified by alkaline treatment with Na_2CO_3

C.D. Lago, H.P. Decolatti, Lucas G. Tonutti, B.O. Dalla Costa, C.A. Querini *

Instituto de Investigaciones en Catálisis y Petroquímica (INCAPE) – FIQ – UNL – CONICET, RN168, Km 0, (3000) Santa Fe, Argentina

ARTICLE INFO

Article history:
Received 11 April 2018
Revised 24 July 2018
Accepted 28 July 2018

Keywords:
H-ZSM-5
Alkaline treatment
Sodium carbonate
Glycerol dehydration

ABSTRACT

Modified H-ZSM-5 zeolite catalysts were studied for the dehydration of glycerol to acrolein in gas phase. The modifications were made by alkaline treatment using Na_2CO_3 solutions in different concentrations, followed by consecutive ion exchanges with NH_4NO_3 solution in order to recover the acidic form of the materials. The mild conditions selected (alkali concentrations, time and temperature) allowed to preserve the crystallinity and framework characteristic in the zeolite, selectively removing silicon while maintaining practically all the aluminum content. This process has important advantages over the alkaline treatment with NaOH (at an equivalent pH), such as high selectivity to remove silicon instead of aluminum, and in addition the yield of synthesized material respect to the initial mass is markedly higher (80% vs 50%). This treatment with Na_2CO_3 solutions leads to multiple positive effects as: increments in the mesoporosity and external surface area; and changes in the nature and accessibility to the acid active sites. The catalytic activity and selectivity were greatly improved. Further, the deactivation by coke deposition was attenuated.

1. Introduction

The particular rise in demand of clean fuels and chemicals obtained from renewable sources has led to an intensive research in order to develop industrial applications of biomass of all types [1,2]. In this sense, one of the most important processes is biodiesel production by transesterification of vegetable oils or animal fats as raw materials. Generally, 10 wt% of glycerol is generated as co-product during biodiesel production, and due to the increase of the biodiesel manufacturing in the last decade, a glycerol oversupply in the global market has occurred, converting this polyol into a very promising low-cost feedstock for the synthesis of value-added specialty and fine chemicals [3]. The price of glycerol has decreased from US$ 0.43 kg^{-1} in 2003 to US$ 0.18 kg^{-1} in 2010 for pure glycerol, and only US$ 0.02 kg^{-1} for crude glycerol [4]. This molecule with three hydroxyl groups can undergo dehydration, oxidation, reforming, hydrogenolysis, etherification and esterification reactions to produce a lot of chemical commodities [5,6]. Dehydration of glycerol produces two important bulk chemicals: 1-hydroxyacetone (acetol) and propenal (acrolein). Acrolein production is currently carried out by partial oxidation of propylene, using mixed metal oxides as catalysts [7]. Therefore, catalytic conversion of glycerol into acrolein offers a cost-effective and sustainable alternative route to replace the present production technology. Acrolein is used for the production of acrylic acid, acid esters, super absorbers polymers, detergents, fragrances, dyes and agrochemicals like methionine, among others products [8,9]. The catalytic conversion of glycerol into acrolein by dehydration can be made in either the gaseous or liquid phase. However, in the liquid phase reaction, the glycerol conversion was limited to 15–20%, to avoid excessive loss of selectivity [10]. Manipulation of conversion and selectivity to acrolein is easier in the gas phase. Several solid acid catalysts such as sulfates, phosphates, and zeolites have been used either in gaseous or liquid phase reactions [11,12]. Other solid acid catalysts as metal oxides [13–15] and heteropolyacids (HPAs) supported on metal oxides [13,16–18] has also been studied in gas phase reaction. The catalytic activity is a function of the textural and acidic properties of the solid. The pore size is a key factor in order to obtain good activity and selectivity. Catalysts with small pores showed lower activity and stability than catalysts with mesopores ranged between 6 and 10 nm [16]. The total amount of acids sites, as well as its strength and nature have a major influence in the performance of the catalysts. In terms of acidity, it has been reasonable established that Brønsted acid sites catalyzes acrolein production [19,20], whereas Lewis acid sites increases the selectivity to hydroxyacetone [21,22]. However, some studies in the literature have proven that

* Corresponding author.
E-mail address: querini@fiq.unl.edu.ar (C.A. Querini).

https://doi.org/10.1016/j.jcat.2018.07.036
0021-9517/

Brønsted acid sites can also catalyze hydroxyacetone production, what occurs when glycerol interacts via the hydroxyl groups attached to primary carbons. Foo et al. [23] demonstrated, using FTIR spectroscopy, a cooperative role of Brønsted and Lewis acid sites in the glycerol dehydration to hydroxyacetone over niobia catalysts. These authors proposed several steps for this reaction. In a first step glycerol is adsorbed on a Lewis acid site, and in a second step it is transformed into 2-propene-1,2-diol, which further tautomerizes to hydroxyacetone The authors concluded that the second step involved the participation of an adjacent Brønsted acid site to generate the 2-propene-1,2-diol.

The zeolites offer several advantages. These solids are environmentally harmless, noncorrosive, thermal and chemical stable and possess a high versatility among other things. Moreover, the shape-selective properties of zeolites related to the presence of an ordered microporous network can restrict the formation of undesired products by control of reactant or product diffusion in the pores as well as the volume available for transition states. Nevertheless, the pure microporous nature of zeolites frequently involves transport limitations, particularly when bulky molecules are involved, which adversely affect catalytic performance. ZSM-5 zeolite is known as a solid acid catalyst for efficient conversion of fossil and biomass resources to fuels and chemicals [24,25]. In addition, ZSM-5 has been observed to exhibit excellent catalytic properties in aromatics compounds synthesis, mainly due to its shape-selectivity characteristic. However, the microporous channels present in its structure may in some cases be a major limitation, because mass transport is slow through these narrow channels, especially when reaction is significantly faster than diffusion in the micropores [26,27]. Scaling down of zeolite crystals from micrometer to nanometer scale and developing mesoporous zeolite catalysts have been recognized as important factors in improving catalytic activity. Emerging mesoporous materials however generally do not comply with most practical requirements as a result of limited thermal stability and poor acidic properties. Consequently, new synthesis procedures for preparation of small zeolitic crystals [28] or post-treatment procedures to create extra-porosity [29] are increasingly investigated. Conventional steaming and acid leaching methods or the less-known treatments in alkaline media have been applied to modify various properties of zeolites. The last method removes preferentially Si from the zeolite framework (desilication) [30], while the former ones lead to dealumination. Desilication was firstly applied to study chemical changes of MFI crystals upon contact with NaOH solutions, and this treatment has shown to induce a significant mesoporosity in MFI-type zeolites [31,32]. Furthermore, this treatment allowed retaining the crystal structure and the acidic properties of the solids. Desilicated zeolites have been investigated in several reactions, including cumene cracking, methanol to propylene, methanol to gasoline, hydroxylation of benzene to phenol, methane aromatization, and hexene conversion [21,33]. In most cases, improved activity, stability, and selectivity have been reported. In general, the observed improvement has been ascribed to enhanced diffusion due to the generation of mesoporous channels. The mesoporous structure is an advantage for the diffusion of reactants because the external surface area of zeolite is improved and the catalytically active acid sites become more easily accessible to reactants.

The versatility of this alkaline treatment opens new avenues to improve diffusion characteristics in zeolite-catalyzed applications. Most of the studies include the use of NaOH in different concentrations, varying the temperature and the time of treatment. If the treatment is very aggressive, although mesoporosity is generated in the structure, changes in morphology can also be produced, with a partial collapse of the zeolite grain. M. Ogura et al. [34] observed changes at micrometric scale combining SEM and TEM techniques, although the changes at molecular or atomic scale were discarded by XRD results. An alternative to prevent this problem is to use a weaker alkali, like Na_2CO_3 [35].

In this paper we present results obtained after modification of an H-ZSM-5 zeolite (Si/Al = 40) by alkaline treatment with Na_2CO_3 aqueous solutions in different concentrations, followed by ionic exchange with NH_4NO_3 to obtain acid catalysts. The textural properties and the acidity of the materials were studied employing numerous characterization techniques. The activity of the solids was tested in the glycerol dehydration reaction to obtain acrolein.

2. Experimental

2.1. Catalyst preparation

A ZSM-5 zeolite with a nominal Si/Al ratio of 40 (CBV-8020), supplied by Valfor in an H-form, was used in this study. The calcined sample of this catalyst is labeled in this work as H-ZSM-5. The alkali treatments were carried out using aqueous solutions of 0.2, 0.3, 0.4, 0.5 and 0.7 mol L^{-1} Na_2CO_3, employing 30 ml of solution per gram of calcined ZSM-5 zeolite. The treatment was carried out with vigorous stirring at 65 °C during 0.5 h, in a flask with a reflux condenser and a water bath, following the procedure previously established for these materials [36]. The zeolite suspension was then cooled down immediately using an ice bath. The remaining product was filtered, carefully washed until neutral pH and finally dried at 100 °C overnight. The alkali-treated samples were obtained in a Na-exchanged form, and it was necessary to convert them into the H-form in order to recover the acidity. After the alkali treatment, two consecutive ion exchanges with 0.5 mol L^{-1} NH_4NO_3 aqueous solutions during 2.5 h in reflux were carried out to each sample. Then, the samples were calcined in air at 550 °C for 2 h. The modified zeolite catalysts were named H-AT (M), being M = 0.2, 0.3, 0.4, 0.5 and 0.7 according to the concentration of Na_2CO_3 used in the alkali-treatment solution.

2.2. Catalyst characterization

Nitrogen adsorption–desorption isotherms were recorded at liquid-nitrogen temperature (−196 °C) and relative pressure (P/Po) interval between 6×10^{-7} and 0.998 in a Quantachrome equipment. Before the adsorption, samples were evacuated at 250 °C during 3 h under vacuum of 1×10^{-5} Pa. The BET model [37] was used in the relative pressure range 0.01–0.10 to calculate the total surface area, while the micropores volume and external surface area were derived from the *t*-plot, according to Lippens and de Boer [38]. The pore-size distribution was calculated employing the Broekhoff and de Boer (BdB) method [39], applied to the adsorption branch of the isotherm.

X-ray diffraction (XRD) patterns were measured in a Shimadzu XD-D1 instrument with a monochromator, CuK_α radiation and a scanning rate of 2° min^{-1} in the range $2\theta = 0°-55°$.

Si and Al concentrations in the filtrate obtained upon alkaline treatment were determined by inductively coupled plasma atomic emission spectroscopy (ICP-OES). Measurements were performed in a Perkin Elmer Optima 2100 DV. Also the Al and Si content in the solids were measured by Energy-dispersive X-ray fluorescence (XRF), using a Shimadzu equipment, model EDX-720, and working in the energy dispersion mode.

The morphology of H-ZSM-5 catalyst before and after the alkaline treatment was studied by Scanning electron microscopy (SEM) samples at 15 KV using an electron microscope (Phenom PROX). In order to ensure that the data collected was representative of the whole sample, scans were made at more than one location, indicating that the zeolite particles are homogeneous.

^{27}Al-MAS-NMR was used to analyze the Al coordination states on the zeolite samples. Spectra were recorded using a Bruker Avance AMX-500 spectrometer. Prior to measurements, all zeolites were stored for 48 h in a desiccator over a saturated $Ca(NO_3)_2$ aqueous solution in order to achieve full pore hydration, thus leading to improved NMR spectral resolution due to minimization of distortions in the Al tetrahedral [40]. After hydration, samples were packed at 42 mbar H_2O into ZrO_2 rotors, which were spun at 10 kHz. $Al(NO_3).9H_2O$ was used as reference. For measuring the 1D spectrum, an excitation pulse with power level of 7 dB and a length of 0.7 μs was applied. Relaxation time was set to 250 ms, and 2400 scans were recorded.

The amount and strength of acid sites were evaluated by pyridine temperature-programmed desorption (TPD). Approximately 10 mg of catalyst, sandwiched by quartz wool, was loaded in a quartz tube. The solids were pretreated in-situ in N_2 flow (30 ml min^{-1}) at 300 °C during 1 h. After cooling down to room temperature, three consecutive saturation steps with pure pyridine were performed. Then, N_2 was flowed and the temperature was increased up to 150 °C, until no physically adsorbed pyridine was detected. The TPD experiments were carried out heating at 12 °C min^{-1} in N_2 flow from 150 °C to 800 °C. Pyridine coming out of the sample cell passed through a methanation reactor. A H_2 stream was also fed to this reactor, quantitatively converting pyridine to CH_4 using a Ni catalyst. The CH_4 was continuously measured by a FID detector.

Pyridine with a diameter of 0.68 nm is at the limit for adsorption in the 10-ring pores of ZSM-5 with a diameter of 5.5 nm. In this case, TPD curves not only depend on the properties of the acid sites, but also on steric limitations of pyridine inside the pores. For this reason, also experiments with adsorption of ammonia were performed in order to analyse the acidity of the catalysts. The samples were pretreated inside the TPD reactor in Ar flow (60 ml min^{-1}) at 300 °C for 1 h, followed by adsorption of ammonia (diluted 1% NH_3 in He) at 100 °C during 45 min. The removal of physically adsorbed ammonia was carried out by purging the sample at 100 °C for 2 h under a flow rate of 60 ml min^{-1} of Ar. Then, TPD of ammonia was performed heating the sample from 100 °C up to 800 °C, at a rate of 12 °C min^{-1}, using the same flow rate of Ar. The amount of desorbed ammonia of each sample was determined by using a mass spectrometer Balzers Omnistar.

The Lewis and Brønsted acidity of the samples was studied by pyridine adsorption followed by infrared spectroscopy (FTIR). Spectral measurements of pyridine adsorption on the samples were performed on a JASCO FT-IR 5300 spectrometer equipped with a DTGS detector. The range and resolution of acquisition were 4600–400 and 4 cm^{-1} respectively. A self-supporting wafer for each sample (~20 mg and 13 mm of diameter) was prepared, placed in a thermostatized cell with CaF_2 windows connected to a vacuum line, and evacuated for 8 h at 400 °C. The background spectrum was recorded first after cooling the sample to room temperature. Afterwards, the solid wafer was exposed to pyridine vapors (Sintorgan, 99% purity) until the system was saturated to 46 mmHg at room temperature; the contact time at this pressure was 12 h. The IR spectrum for each sample was obtained after pyridine desorption by evacuation for 1 h at 100, 200, 300 and 400 °C. All the spectra were recorded at room temperature before and after pyridine adsorption and desorption at each temperature. The difference spectrum was finally obtained by subtracting the background spectrum previously recorded.

The coke in the catalysts after reaction was characterized by temperature-programmed oxidation (TPO). The gases coming out of the sample cell passed through a methanation reactor, as in the pyridine TPD experiments, but in this case the CO and CO_2 resulting from coke oxidation were converted to CH_4. Again, this compound was continuously measured using a FID detector. Under the experiment conditions (400 °C, 6% O_2, 40 ml min^{-1} H_2 flow), a 100% conversion of CO_x was reached and in this way the sensitivity of the technique was greatly improved. The analysis was carried out with a heating rate of 12 °C min^{-1} starting from 20 °C. Equipment calibrations were made using pulses of CO_2 diluted in He.

2.3. Catalyst performance tests

The dehydration of glycerol was conducted at atmospheric pressure in a continuous fixed-bed stainless steel reactor, using 0.4 g of catalyst (particle size 40–80 mesh) without diluents. Prior to the catalytic tests, catalysts were pretreated at 300 °C in N_2 flow for 1 h to remove adsorbed water. The reaction feed was an aqueous solution containing glycerol (20 wt%). It was evaporated in a preheater at 260 °C, with 50 ml min^{-1} of N_2 as carrier gas. It is well known that diffusion is driven by the concentration difference between internal and external space of catalyst [41]. Y. Gu et al. studied the effect of carrier gas, concluding that the glycerol conversion and acrolein selectivities were improved when using carrier [42]. The authors stated that the introduction of carrier gas could enlarge the concentration difference by supplying glycerol (and removing products) continuously to (and from) outer space of catalyst, which could stimulate the diffusion of glycerol into channels and products out of channels of H-zeolites. Besides, the dilution effect of carrier gas decreases the partial pressures of reactants and products simultaneously, which reduce the rates of coke formation and catalyst deactivation. In addition, a lower glycerol partial pressure could also reduce the possibility of intermolecular dehydration, which would kinetically affect the catalyst performance.

Throughout this work, the space velocity used (WHSV = 0.75 h^{-1}) represents the mass of glycerol per gram of catalyst, per hour. The reactor was placed in an electrically heated furnace, and the reaction temperature was set at 275 °C. After the reaction, the carrier flow was maintained for 1 h, in order to purge the system. Reaction products together with the unconverted glycerol were collected in a cold trap maintained at 5 °C at 30 min intervals. The analysis of the products was carried out offline in an Agilent 7820A gas chromatograph (GC) equipped with a HP-FFAP capillary column (30 m × 0.32 mm × 0.25 μm) and a flame ionization detector (FID). The following products have been identified and quantified: acrolein, acetaldehyde, propanal, acetol, and methanol. Others compounds in low concentrations have not been identified. The following equations were used to calculate glycerol conversion, product yield, selectivity and the relative deactivation:

$$\text{Glycerol conversion}\,(\%) = \frac{\text{moles of glycerol reacted}}{\text{moles of glycerol fed}} \times 100 \quad (1)$$

$$\text{Product yield}\,(\quad) = \frac{\text{moles of product}}{\times\ \text{moles of glycerol fed}} \times 100 \quad (2)$$

$$\text{Product selectivity}\,(\quad) = \frac{\text{product yield}}{\text{glycerol conversion}} \times 100 \quad (3)$$

$$\text{D}\,(\quad) = \frac{X^{\circ} - X}{X^{\circ}} \times 100 \quad (4)$$

The coefficient ν represents the number of moles of a given product obtained per mole of glycerol, being 1.5 for acetaldehyde and 1 for all the other products. In Eq. (4), D(%) is the percentage of deactivation, calculated using the initial (X°) and final (X) glycerol conversion.

Also, experiments varying the WHSV (1.5 h^{-1} and 3 h^{-1}) or the temperature (300 °C) were carried out, in order to study the deactivation phenomena on the catalysts and the products distribution.

3. Results and discussion

3.1. XRD analysis

Fig. 1 shows the XRD patterns for the calcined H-ZSM-5 zeolite and for the different catalysts obtained after the alkaline treatments. The changes in crystallinity of the desilicated zeolite were calculated based on the relative intensities of the reflection peak at 23° (2θ), taking the crystallinity of the parent sample to be 100%. No appreciable changes were observed in the treated samples, which showed crystallinity values ranged between 98% and 100%. The diffraction peaks assigned to MFI type materials did not change in intensity and also the lattice parameters were the same after alkali-treatment. Therefore, X-ray diffraction analysis confirmed the preservation of the long-range crystal ordering in the samples after the alkali treatment.

Ogura et al. [34] observed that the peaks at 23.07° and 23.25°, respectively assigned to [0 5 1] and [−5, 0, 1] of MFI, were distinctly splitted after alkali-treatment with NaOH, indicating that poor crystallinity parts of ZSM-5 were selectively dissolved. However, this change was not observed in this work.

It is important to mention that the desilication by alkali treatment with Na_2CO_3 produces lower modifications in the zeolite framework in comparison with that observed in a previous work when NaOH was employed as the alkali [43] and also as was reported by others authors [44]. For example, in the case of treating an H-ZSM-5 (Si/Al = 15) with a 0.8 mol L^{-1} Na_2CO_3 solution, Le Van Mao et al. [35] reported a 92% of crystallinity in the modified zeolite.

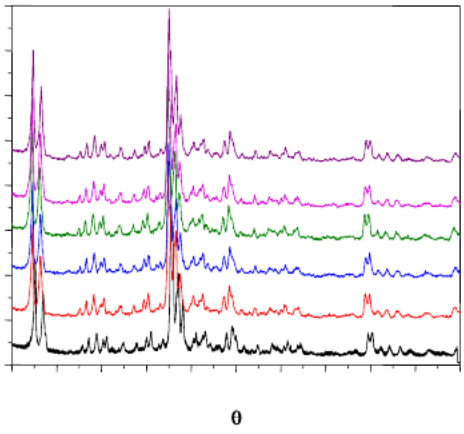

Fig. 1. XRD patterns of original zeolite (a) H-ZSM-5 and after alkaline treatment (b) H-AT(0.2), (c) H-AT(0.3), (d) H-AT(0.4), (e) H-AT(0.5) and (f) H-AT(0.7).

3.2. SEM analysis

SEM analysis showed that the zeolite particles size is in the range of 0.5–2 μm. All catalysts consist of similar particles associated with small crystallites and large agglomerated crystals, as other researchers previously observed [34]. After the alkali treatment, no visually detectable changes in the general morphology of the particles were observed (see Supplementary Data, Fig. S1). The particles of the alkaline-treated sample have a slightly rougher surface.

Supplementary data associated with this article can be found, in the online version, at https://doi.org/10.1016/j.jcat.2018.07.036.

3.3. Textural properties

Fig. 2A shows the N_2 adsorption-desorption isotherm of the original H-ZSM-5 (curve a). It is a type I isotherm with an initial slope due to the adsorption in the micropores of the zeolite, and then a plateau at high relative pressure. The presence of a type H4 hysteresis loop was observed, associated to slit-shaped mesopores which coexist with the micropores [35,44,45]. These mesopores are not cylindrical, and represents an external surface area of 150 m^2 g^{-1} (Table 1).

After the alkali treatment, the isotherms (curves b–f) practically did not change in the relative pressure region below $P/P^o = 0.3$, indicating the preservation of the microporous structure of the material. The micropores volume decreased slightly in comparison to the non-treated zeolite, but their values hardly changes among the different alkali concentrations (Table 1).

At higher relative pressure, the amount of adsorbed N_2 increased in the alkaline treated samples, and the hysteresis loop was modified, indicating in this case the generation of mesoporosity in the solids [46]. This phenomenon is more appreciable when the intensity of the alkali treatment was increased. To facilitate the comparison the isotherm of the non-treated H-ZSM-5 zeolite was copied (dashed line) over imposing it with the isotherms of the modified catalysts (curves b and f) in Fig. 2A. It can be observed that the mesopores volume and external surface area were improved in all cases.

In addition, some enlargement of the existing mesopores in the parent material was also observed through the broadening of the hysteresis loop given by the N_2 adsorption desorption isotherms as indicated in Fig. 2A.

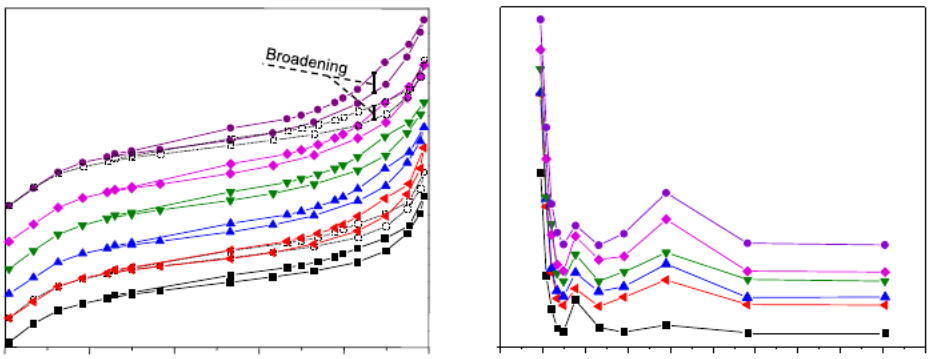

Fig. 2. (A) N_2 adsorption-desorption isotherms (vertically shifted for better observations) and (B) Pore size distribution; for samples (a) H-ZSM-5 (b) H-AT(0.2), (c) H-AT(0.3), (d) H-AT(0.4), (e) H-AT(0.5) and (f) H-AT(0.7).

Table 1
Textural properties, XRF and ICP results.

Sample	S_{BET} ($m^2 g^{-1}$)	S_{EXT} ($m^2 g^{-1}$)	$V_{microp.}$ ($cm^3 g^{-1}$)	$V_{mesop.}$ ($cm^3 g^{-1}$)	Si/Al[a]	%Al[b] extracted	%Si[b] extracted
H-ZSM-5	406	150	0.130	0.137	41.3	–	–
H-AT(0.2)	384	163	0.113	0.159	36.0	0.20	5.7
H-AT(0.3)	392	168	0.114	0.168	34.6	0.17	6.9
H-AT(0.4)	421	195	0.116	0.180	34.3	0.15	6.7
H-AT(0.5)	417	188	0.117	0.185	33.6	0.13	8.2
H-AT(0.7)	416	183	0.119	0.190	32.4	0.16	8.4

[a] Obtained by XRF analyses of the solids.
[b] Obtained by ICP analyses of the filtrate.

Fig. 2B shows the pore size distribution obtained after applying the BdB method to the N_2 adsorption isotherms. For the H-ZSM-5 zeolite, the presence of mesopores with a narrow size distribution around 35 Å was detected. After the alkali treatment, a small decrease in the amount of these mesopores was observed, probably because some of them increased its size. However, the major change in the pore size distribution is the generation of new pores with a broad size distribution around 78 Å. An increase in the concentration of Na_2CO_3 for the alkali treatment produced more quantity of these mesopores.

In all samples, an increase of the external surface due to the mesoporosity generation was observed, with a slowly decrease of the micropores volume (Table 1). However, it is interesting to analyze that when a low concentration of the alkali was employed, the total BET surface area was reduced in comparison with the non-treated zeolite. A reason for this could be the pore blockage by deposition of different species. For example, silicon species dissolved from the zeolite framework precipitated easily on the surface of the crystals, forming an amorphous silica layer [47]. This was observed by other authors when using low NaOH concentrations and low contact time that correspond to mild treatments conditions [34]. However, in our case, the presence of amorphous silica in the prepared materials is rule out according to the XRD results and the crystallinity values obtained. For the samples treated with alkali concentrations of 0.4 mol L^{-1} or greater, the increase of the external surface was more appreciable, and also the BET surface was improved. In this case, the higher concentration of CO_3^{-2} leads to a more extensive hydrolysis of these species and the formation of OH^{-1} ions, which are capable of removing silicon, preventing the precipitation and blockage of the pores.

There is another possible reason for the reduction of the BET area when Na_2CO_3 is used as alkali, related to the deposition of CO_3^{-2} species which are not removed by calcination and could be responsible of a possible total or partial pore blockage, as discussed in the next section.

3.4. FTIR analysis

Fig. 3 shows the FTIR results in the 800–1800 cm^{-1} region for the original H-ZSM-5 zeolite and for the samples after the alkaline treatment. New signals associated to carbonate species appear in the modified catalysts (curves b–f). In these spectra the signal at 1560 cm^{-1} corresponds to the CO_3^{-2} asymmetric stretching (from pure Na_2CO_3), while the doublet at 1490–1440 cm^{-1} is related to the CO_3^{-2} asymmetric stretching also, but when this specie is attached to Al^{+3} atoms ($Al(OH)_3 + Na_2CO_3$). No appreciable changes in the intensity of the signals were observed, therefore according to this technique the amount of deposited species would be similar for all the samples. Su et al. [48] observed these signals, when they studied carbonate species adsorbed on aluminum and iron oxides, employing in situ infrared experiments.

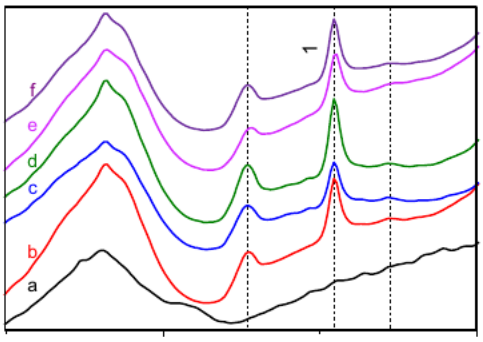

Fig. 3. FTIR spectra of the samples (a) H-ZSM-5, (b) H-AT(0.2), (c) H-AT(0.3), (d) H-AT(0.4), (e) H-AT(0.5) and (f) H-AT(0.7).

3.5. Si and Al removal during the alkaline treatments

The effectiveness of the alkali treatment for selectively removing Si and maintaining the Al content was analyzed by XRF measurements in the solids, and ICP determinations in the filtrate. Table 1 resume the Si/Al ratio which was reduced from 41.3 in the non-treated zeolite H-ZSM-5 to 36 in the H-AT(0.2). Then, for the other samples, only a slight decrease of this parameter with the alkali concentration was observed, being the percentage of reduction of the Si/Al ratio between 16 and 21%.

When the alkali treatment was conducted under the same conditions to an H-ZSM-5 with lower silicon content (Si/Al = 15), there were no appreciable changes in the value indicating that the treatment with Na_2CO_3 was not effective for this Si/Al ratio (result not shown). In a previous work, it was shown that when the treatment for this zeolite was conducted using NaOH 0.2 mol L^{-1}, a decrease in the Si/Al ratio of 8.5% was observed [43]. Le Van Mao et al. [35] reported a reduction of 48% in a similar zeolite, but the authors used more aggressive treatment conditions: three consecutive treatments with Na_2CO_3 0.8 mol L^{-1}, higher temperature (80 °C) and more contact time (4 h). After comparing the results obtained for an H-ZSM-5 (Si/Al = 15) with those observed for a Na-Y (Si/Al = 2.4) and a Na-X (Si/Al = 1.2), they concluded that with higher Si/Al ratio in the material, the alkaline treatment was more effective.

Particularly for H-ZSM-5 zeolites, the optimum Si/Al ratio to carry out the treatment is ranged between 25 and 50. When the Si/Al ratio is lower than 25, the desilication is not effective due to a stabilizing effect of the aluminum in the framework [49,50].

The ICP results obtained in the analyses of the Si and Al contents in the filtrate are also reported in Table 1. It can be noticed that the amount of extracted aluminum from the zeolite was very low, around 0.2% of the initial content. Instead, the percentage of silicon removed was 8.4% for the sample H-AT(0.7). This is a clear evidence of the high selectivity of the treatment with sodium carbonate regarding the removal of Si compared to Al.

3.6. ^{27}Al-MAS-NMR results

The normalized ^{27}Al-MAS-NMR spectra for all the samples are shown in Fig. 4. The signal at 55 ppm indicates the presence of tetrahedral coordinated framework Al (FAL). The peak shape is narrow and symmetric and the intensities were comparable for all samples. No signals of dealumination were detected after the alkaline treatment. Also the signal at −0.55 ppm was observed, which corresponds to the presence of octahedral non framework Al (EFAL) [51]. Patterns recorded for the non-treated and alkaline-treated H-ZSM-5 zeolites have shown to be very similar, with a negligible contribution from non-framework aluminum species. This suggests that the aluminum was predominantly tetrahedrally coordinated in the zeolite framework upon the alkaline treatment with Na_2CO_3. Similar results were reported by others authors when performed ^{27}Al-MAS-NMR experiments to H-ZSM-5 zeolite modified by alkaline treatment with NaOH [36].

It can be concluded that the conditions adopted in this work for the alkali treatments were quite moderate, the removal of Si was highly selective, the generation of mesoporosity was appreciable, and the crystalline structure of the zeolite was not altered.

3.7. Anion effect: comparison of NaOH and N_2CO_3 during the alkaline treatment

In the case of the Na_2CO_3 solutions used in this work to perform the alkaline treatments, the pH is close to 12 in all cases, due to the buffer characteristics of these solutions.

In order to evaluate the effect of the anion present in the alkali (OH^- or CO_3^{-2}), the H-ZSM-5 zeolite was treated with a 0.01 mol L^{-1} NaOH solution, which has the same pH than the Na_2CO_3 solution (pH = 12). The results were compared with those obtained for the sample H-AT(0.5), because the 0.5 mol L^{-1} Na_2CO_3 has the pH closer to 12 (pH = 12.009). The percentage of Si and Al extracted when using NaOH were 0.83% and 0.35% respectively. Instead, by using Na_2CO_3 the values were 8.2% of Si and 0.13% of Al in the sample H-AT(0.5) (Table 1). Accordingly, at equivalent pH values, the NaOH removes only 10% of the Si extracted with Na_2CO_3. Furthermore, the NaOH solution removes 69% more Al from the framework, which affects negatively the final acidity of the materials.

This is a very important difference between these two bases. In summary, using the alkaline treatment with Na_2CO_3, the extraction of silicon is maximized with a minimum loss of aluminum.

On the other hand, it is very important to remark, that the recovery of the starting material after the alkaline treatment with Na_2CO_3 was 80%, whereas only 50% of the initial mass was recovered when the treatment was carried out with NaOH. Consequently, due to a better desilication performance, and a lower loss of the starting material (i.e. better yield), the treatment with Na_2CO_3 is advantageous.

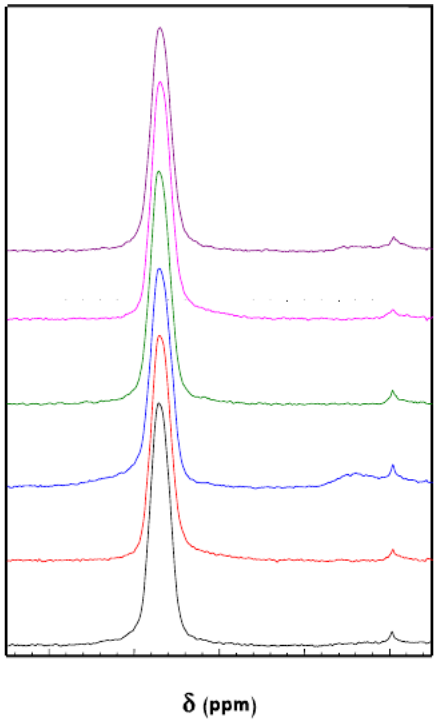

Fig. 4. ^{27}Al-MAS-NMR spectra samples (a) H-ZSM-5 (b) H-AT(0.2), (c) H-AT(0.3), (d) H-AT(0.4), (e) H-AT(0.5) and (f) H-AT(0.7).

3.8. Acidic properties

Information about the superficial acidity of the solids was obtained by Pyridine and Ammonia TPD, and by FTIR experiments.

Fig. 5A shows the Pyridine TPD profiles. The area under the curves is related to the total amount of acid sites, whereas the peaks desorption temperatures indicate the strength of these acid sites. The original zeolite H-ZSM-5 (curve a) showed a profile with two peaks, one at low temperature (240 °C) corresponding to weak acid sites and another centered at 610 °C associated to strong acid sites. A total acidity of 0.37 mmol g^{-1} was detected for this material, being 90% strong acid sites.

After the alkali treatment, some modifications were observed in the acidic properties. First, in all cases, the amount of weak acid sites decreased. Only the sample H-AT(0.4) showed sites with weak acidity, while very low amount of weak acid sites were detected for the other samples.

The position of the peak at higher temperature was slightly moved to lower temperature in the case of the samples H-AT (0.2), H-AT(0.3) and H-AT(0.4). Instead, for the samples treated with higher concentration of alkali, H-AT(0.5) and H-AT(0.7), the position for the maximum was maintained without changes as compared to the untreated catalyst.

Table 2 summarized the acidic values of the catalysts. The amount of total acid sites determined by pyridine TPD analyses was notably increased for the treated samples in comparison with the non-treated zeolite, and the generated acid sites had mainly high strength, as shown in the pyridine TPD profiles.

In conclusion, the total amount of acid sites determined by pyridine TPD analyses was higher in the zeolite after the alkaline treatment. The strength and amount of the acid sites were comparable between the modified zeolites, but the samples H-AT(0.5) and H-AT(0.7) presented the stronger acidity.

As a result of the preferential silicon extraction, the Si/Al ratio in the treated zeolite was lower than in the non-treated sample and thus the number of potential Brønsted acid sites per unit weight should be increased.

Fig. 5B shows the Ammonia TPD results for the untreated material and for the samples H-AT(0.2) and H-AT(0.7). In this case, the TPD profiles were similar, indicating that the strength and total amount of acid sites in the modified samples were similar to the original H-ZSM-5. Similar results were obtained for the samples H-AT(0.3), H-AT(0.4) and H-AT(0.5) (not shown). The acidic values obtained by NH_3 TPD for the modified samples (not shown) are in agreement with those obtained using pyridine. It is clear that the size of the ammonia molecule allowed the accessibility to all the acid sites in the zeolites, also in the original H-ZSM-5 catalyst. For the pyridine results, the differences in total acidity between the untreated zeolite and the modified materials was due to the mesoporosity generated by the alkaline treatment, which facilitate the accessibility of the pyridine to the acid sites.

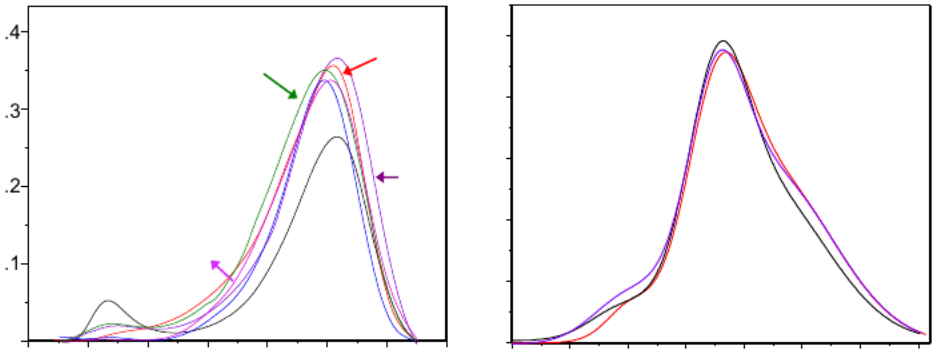

Fig. 5. (A) Pyridine TPD profiles (a) H-ZSM-5, (b) H-AT(0.2), (c) H-AT(0.3), (d) H-AT(0.4), (e) H-AT(0.5) and (f) H-AT(0.7). (B) Ammonia TPD profiles (a) H-ZSM-5, (b) H-AT(0.2) and (f) H-AT(0.7).

Table 2
Acidic results.

Sample	Acidity (mmol g^{-1})[a]	B/L[b]
H-ZSM-5	0.37	0.53
H-AT(0.2)	0.48	1.86
H-AT(0.3)	0.43	2.61
H-AT(0.4)	0.47	2.10
H-AT(0.5)	0.45	2.62
H-AT(0.7)	0.43	2.04

[a] Obtained from pyridine TPD results.
[b] Obtained from pyridine FTIR results.

The nature of the acid sites was investigated using the Pyridine FTIR technique. Fig. 6A shows the signals associated to chemically adsorbed pyridine in the range 1700–1400 cm^{-1} after evacuation at 100 °C. The non-treated zeolite H-ZSM-5 (curve a) displayed the bands characteristic of pyridine adsorbed on Lewis acid sites at 1622 and 1450 cm^{-1} (L), the bands attributed to Brønsted acid sites at 1544 and 1636 cm^{-1} (B), and the signal corresponding to pyridine adsorbed on both Lewis and Brønsted acid sites at 1490 cm^{-1} (L + B) [52].

For the alkaline treated zeolites (curves b–f), there was a very important increase in the total intensity of the FTIR signal, in comparison with the non-treated zeolite. This is in agreement with the pyridine TPD results. The non-treated H-ZSM-5 zeolite presented mainly Lewis acid sites (B/L = 0.53). In addition, a pyridine FTIR analyses with thermo-desorption at different temperatures was performed. Fig. 6B shows results obtained with the non-treated H-ZSM-5 zeolite. It can be observed that the intensity of the Lewis acid sites signal for this material was too weak and practically it disappears after evacuation at 200 °C (curve b), while a small amount of Brønsted acid sites remains after evacuation at 400 °C (curve d). The Brønsted acid sites in the H-ZSM-5 were more thermally stable. Therefore, it can be concluded that the low temperature peak in the pyridine TPD profile (Fig. 5, curve a) represents weak Lewis acid sites, and the high temperature range corresponds mainly to Brønsted acid sites. This assignment to the regions in the TPD profile with the nature of the acid sites is valid also for the treated zeolites.

The pyridine FTIR spectra for the zeolite modified by alkali treatments followed by two ion exchange steps with NH_4NO_3 solution (Fig. 6A, curves b–f) showed an important increase in the size of the signal at 1544 cm^{-1}. This result indicates that the concentration of framework Al (FAL) sites on the surface of the treated samples was enhanced; and consequently the concentration of Brønsted acid sites was improved. This is because the greater

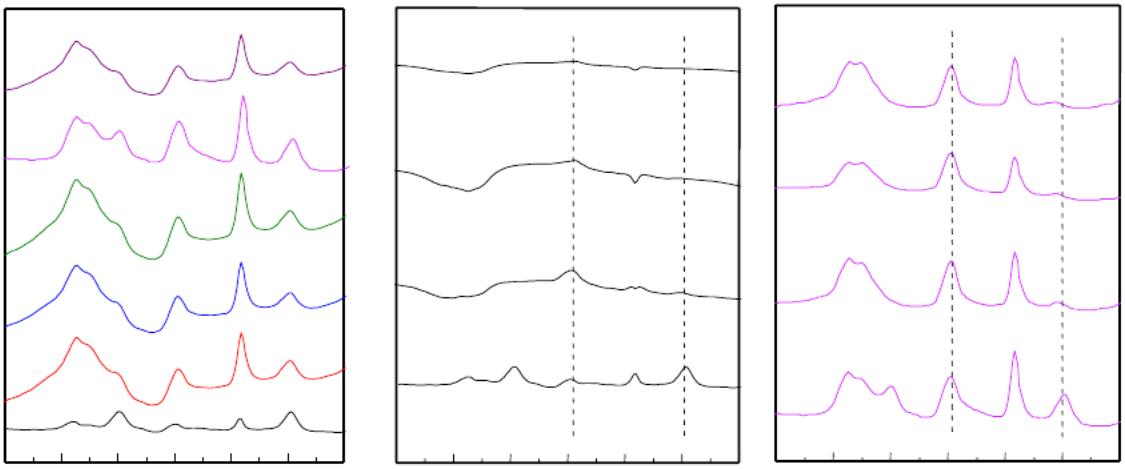

Fig. 6. Pyridine FTIR spectra. (A) After desorption at 100 °C for the catalysts (a) H-ZSM-5, (b) H-AT(0.2), (c) H-AT(0.3), (d) H-AT(0.4), (e) H-AT(0.5) and (f) H-AT(0.7). (B) For the H-ZSM-5 sample after desorption at (a) 100 °C, (b) 200 °C, (c) 300 °C and (d) 400 °C. (C) For the H-AT(0.5) sample after desorption at (a) 100 °C, (b) 200 °C, (c) 300 °C and (d) 400 °C.

external surface area and mesoporosity obtained upon the alkaline treatment, led to a higher exchange of NH_4^+ that were transformed in H^+ by calcination. Fig. 6C shows the pyridine FTIR results for the sample H-AT(0.5) after evacuation at different temperatures. These results demonstrate that the Brønsted acid sites are strong, maintaining adsorbed pyridine even after evacuation at 400 °C.

The concentrations of Brønsted and Lewis acid sites were estimated from the intensities of the band at 1544 and 1450 cm^{-1} respectively in Fig. 6A, following the procedure of Emeis [53]. These values were used to calculate the B/L ratio for all the samples (Table 2). These results showed a higher concentration of Brønsted acid sites accessible to pyridine on the treated samples. These Brønsted sites were proposed as the catalytic species where the dehydration of glycerol to acrolein takes place [20].

It is very important to highlight the high strength of the Brønsted acid sites in the H-AT(0.5) treated zeolite, that are able to maintain the pyridine adsorbed even after the treatment at 400 °C (Fig. 6C). On the other hand, the original zeolite showed a decrease in the amount of pyridine adsorbed as a function of the desorption temperature in the range 100–400 °C, as indicated in Fig. 6B. This different strength of the acid sites explains the lack of a direct correlation between the Si/Al ratio and the amount of acid sites quantified by pyridine TPD in each catalyst. The pretreatment at 150 °C carried out during this analysis, proportionally desorbs more pyridine from the weaker acid sites of the original zeolite, thus detecting a significant lower acid sites density compared to the zeolite treated with the sodium carbonate.

3.9. Activity results

3.9.1. Reaction network discussion

Fig. 7 shows a complete reaction scheme adapted from Corma et al. [8] based on the findings of the present work, including the main products. Glycerol can participate in numerous consecutive and parallel reactions as dehydration, cracking, and hydrogen transfer, all of them catalyzed by acid sites. In addition to acrolein, others oxygenated compounds produced by glycerol conversion are acetaldehyde, and hydroxyacetone (acetol). Acetone, propanol and methanol were detected in trace amounts. A number of heavier unidentified compounds were found, defined as "others". Acetals, which are formed by the reaction between glycerol and acrolein, are included within this group of unknown products.

Dehydration of glycerol has been shown to first produce acetol and acrolein [54]. Two distinct and independent pathways occurs, one leading to acrolein through 3-hydroxypropenal (a very unstable product) and the other forming acetol. The first pathway implies the removal of the central alcohol function in the glycerol molecule, whereas the second implies the removal of one of the two terminal alcohol groups. This mechanism has been observed on a wide variety of catalysts, including base and acid-supported catalysts and zeolites [13,16]. The predominant route depends mainly on the nature of the acid sites. The mechanism for the formation of acrolein over Brønsted acid sites has been previously suggested, as well as the reaction to acetol over Lewis acid sites [17]. As it was mentioned in the introduction section, a cooperative role of Brønsted and Lewis acid sites in the glycerol dehydration to acetol is also possible [23].

Acetone can be obtained from the hydrodeoxygenation of acetol and acetaldehyde is presumably derived from the catalytic decomposition of the feed [16]. Corma et al. [8] found that acetaldehyde can also be formed from acetol, and proposed a mechanism for acetaldehyde formation via hydrogen-transfer mechanism, with a dehydrogenated dione intermediate. This intermediate can also form propanal [8].

Witsuthammakul and Sooknoi [55], and previously Chai et al. [13] reported that acrolein is highly reactive and it can undergo secondary reactions such as condensation and oligomerization, forming high molecular weight products, namely as "others". These products are cyclic unsaturated and oxygenated compounds such as phenol, dihydrofuran, cyclopentenone, methyl cyclopentenone and cyclohexenone. They are responsible for coke formation and cause the catalyst deactivation, particularly in large pore zeolites [56]. Kim et al. reported XRD results indicating that the carbon deposited on the catalyst surface exist as amorphous species [57]. It was found that the strong acid sites led to low acrolein selectivity due to a fast coke deposition [13].

It is also known that glycerol can form oligomers (polyglycerols), which may lead to coking reactions [58]. The same mecha-

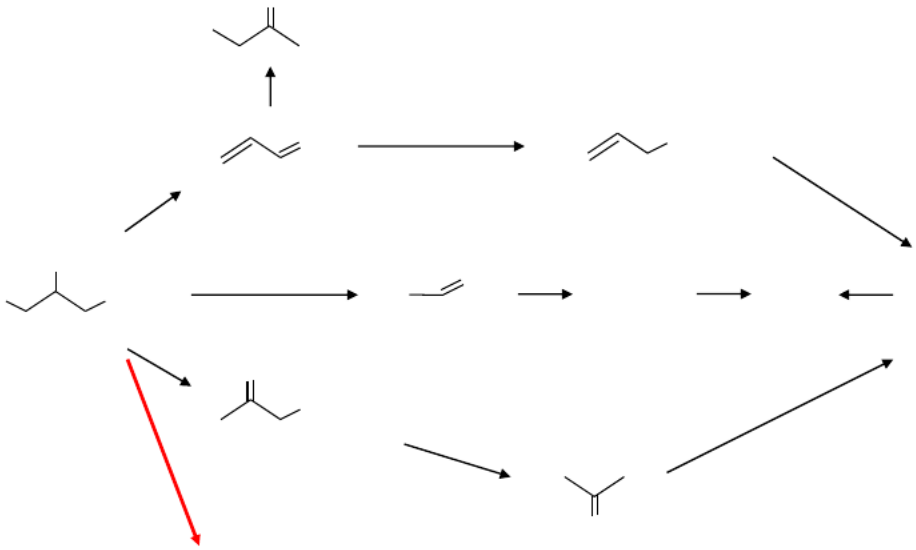

Fig. 7. Scheme of reaction for glycerol dehydration.

nism is applicable to acetol as well. Coke is also formed from acetaldehyde [59], and probably acrolein; coke can be formed from many sources.

3.9.2. Catalytic results

Fig. 8 shows the catalytic activity results obtained at a space velocity WHSV = 0.75 h^{-1} and 275 °C. The glycerol conversion as a function of time on stream (TOS) is showed in Fig. 8A. A decrease in the conversion with time on stream was observed in all cases, due to the deactivation by coke formation, which is the main cause of deactivation during glycerol dehydration with solid acids [60]. The TPO profiles of deactivated catalysts were similar and the percentage of carbon deposits after 7 h of reaction was around 11 wt% in all samples. Fig. 9 shows the TPO results for the H-ZSM-5, H-AT (0.5) and H-AT(0.7).

After 7 h of time on stream the conversion obtained with the H-ZSM-5 zeolite felt below 50%. In the case of the alkaline treated zeolites the stability was much better, being the conversion close to 70% at the same time on stream. It is also observed that in the case of the original zeolite the conversion continues decreasing, while it tends to stabilize in the modified catalysts. Possibly, the deactivation by blocking the mouth of pores with coke is more important in the original zeolite. The higher conversion reached for the treated zeolites is associated to the higher amount of accessible acid sites obtained on these solids. The availability of more active sites allows conversions of practically 100% up to TOS of 3 h, while at the same time the conversion for the non-treated zeolite was below 80%. The changes in the selectivity during the first hours of the reaction indicate that in spite of maintaining the conversion in 100%, deactivation by coke deposition is taking place.

The increased mesoporosity, also attenuates the catalyst deactivation by coke formation. The geometry of channels and the intracrystalline diffusivity have great impact on the formation of coke [42]. The samples H-AT(0.5) and H-AT(0.7) which were synthesized with the greater external surface area and the narrowed pore size distribution, showed the better stability in reaction (70% Conversion at TOS = 7 h). The relative deactivation calculated according to Eq. (4) were: 49.4%, 35.6%, 36%, 34.8%, 30.2% and 31.1% for samples H-ZSM-5, H-AT(0.2), H-AT(0.3), H-AT(0.4), H-AT(0.5) and H-AT(0.7) respectively.

Besides, Fig. 8B shows that the selectivity to acrolein was also improved for the treated zeolite. Initial selectivities (TOS = 1 h) close to 75% were obtained, well above the 50% reached for the non-treated material. The nature and strength of the acid sites plays a fundamental role in the acrolein selectivity. It was proposed that the Brønsted acid sites were more active than the Lewis acid sites to convert glycerol to acrolein [13]. In these catalysts,

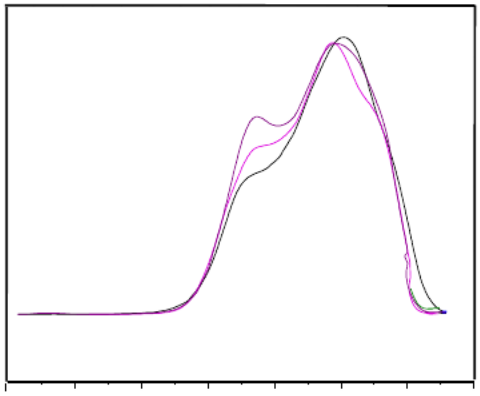

Fig. 9. TPO profiles for catalysts after activity tests. (a) H-ZSM-5, (b) H-AT(0.5) and (c) H-AT(0.7).

there is also a correlation between these variables, since the pyridine FTIR results previously discussed showed a higher B/L ratio in the treated zeolites and accordingly an improvement in the selectivity to acrolein was obtained.

3.9.3. Effect of temperature and space velocity

Fig. 10 shows the glycerol conversion and acrolein selectivity with TOS obtained for the catalysts H-ZSM-5 and H-AT(0.7) at 275° C and different space velocities. It can be seen that the catalytic behavior is better for the modified zeolite at each spatial velocity. If each catalyst is analyzed separately, it is clear that an increase in the feed rate to the reactor produces a much more pronounced deactivation of the material.

Although acrolein is one of the primary products of glycerol dehydration, as discussed in Section 3.9.1, if the selectivities values are compared at TOS = 1 h, it is observed that an increase in the space velocity produce a decrease both in the glycerol conversion and in the selectivity to acrolein. It is important to observe that this correlation (at lower conversion, lower selectivity to acrolein) occurs for different catalysts at a given space velocity (see Fig. 8) or comparing data obtained at different space velocities and different catalysts (Fig. 10). For example, after 5 h on oil, where the catalytic behavior is rather stable, at a given TOS the selectivity decreases as the conversion decreases. Therefore, glycerol is involved in parallel reactions that lead to the formation of other compounds decreasing the selectivity to acrolein at low conver-

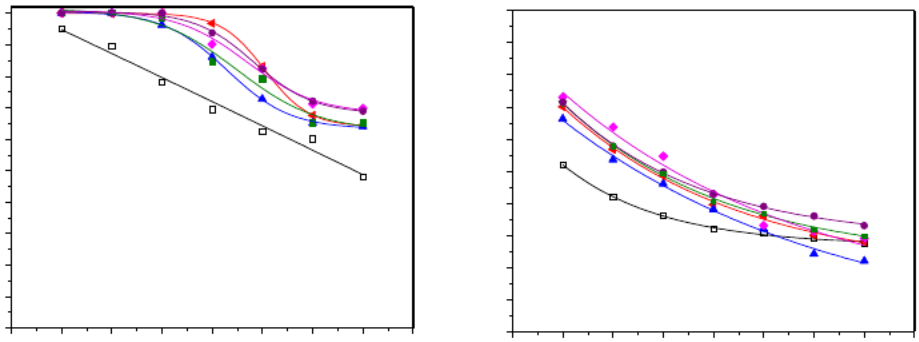

Fig. 8. (A) Glycerol conversion and (B) Acrolein selectivity with time on stream at WHSV = 0.75 h^{-1} and T = 275 °C for the catalysts: (□) H-ZSM-5, (◀) H-AT(0.2), (▲) H-AT (0.3), (■) H-AT(0.4), (♦) H-AT(0.5), (●) H-AT(0.7).

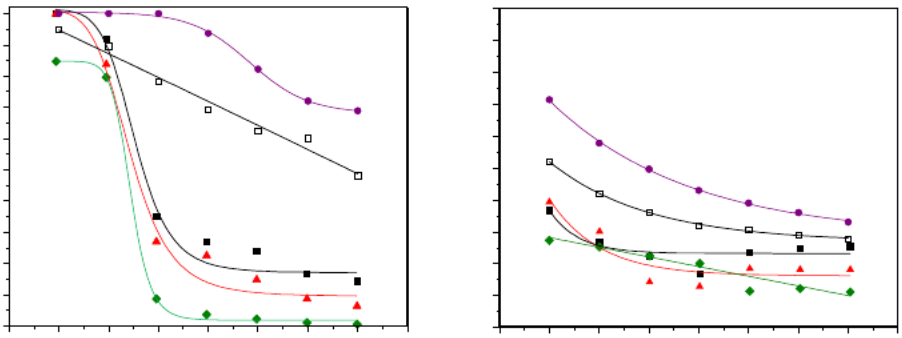

Fig. 10. (A) Glycerol conversion and (B) Acrolein selectivity at T = 275 °C with time on stream at different WHSV. H-ZSM-5 (□ = 0,75 h^{-1}, ♦ = 3 h^{-1}) and H-AT(0.7) (● = 0,75 h^{-1}, = 1,5h^{-1}, ▲ = 3 h^{-1}).

Table 3
Glycerol conversion and products selectivity at T = 275 °C and WHSV = 0.75 h^{-1}.

Sample	H-ZSM-5		H-AT(0.2)		H-AT(0.3)		H-AT(0.4)		H-AT(0.5)		H-AT(0.7)	
TOS	1 h	7 h	1 h	7 h	1 h	7 h	1 h	7 h	1 h	7 h	1 h	7 h
Glycerol conversion (%)	95	48	100	64.4	100	64	100	65.2	100	69.8	100	68.9
Acrolein yield (%)	53	13	70	18.0	66	14.1	72	19.6	74	20.2	72	22.7
Selectivity (%)												
Acetaldehyde	3.8	2.43	4.3	1.5	4.5	1.76	4.3	1.1	5.0	1.8	5.0	1.87
Propanal	3.0	0.88	3.7	0.82	3.8	1.16	3.3	0.73	4.0	0.84	4.7	1.0
Acetol	15	15.2	15	16.1	18	19	16	17	15	16	15	15.8
Acrolein	53	27.7	70	28	66	22	72	30	74	29	72	33
Others	25.2	53.1	6.7	53.1	7.2	55.3	4.4	50.7	2.5	51.6	3.4	47.4

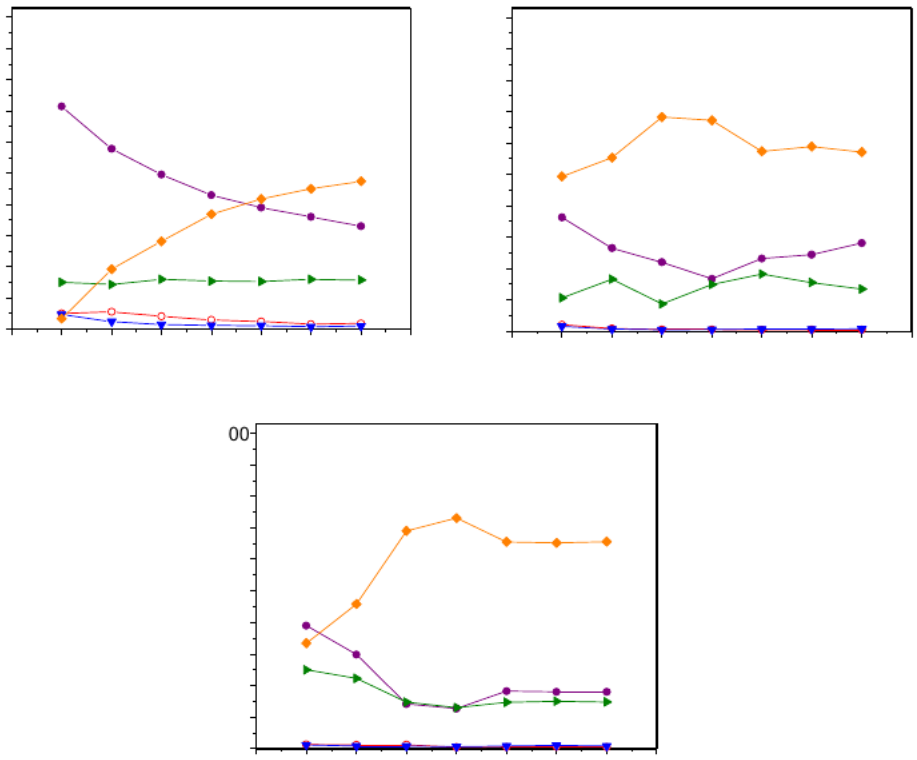

Fig. 11. Product distribution at different WHSV for H-AT(0.7) catalyst at 275 °C. Acrolein (●), acetaldehyde (○), propanal (▼), acetol (▶), others (◆).

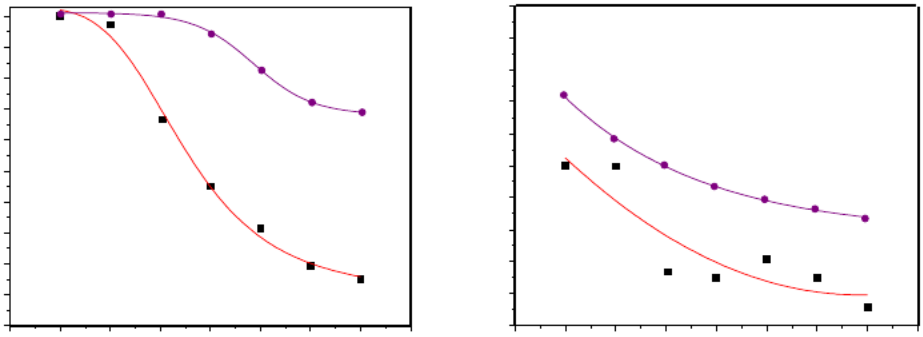

Fig. 12. (A) Glycerol conversion and (B) Acrolein selectivity with time on stream at WHSV = 0.75 h^{-1} for the catalysts H-AT(0.7) at: T = 275 °C ( ), T = 300 °C ( ).

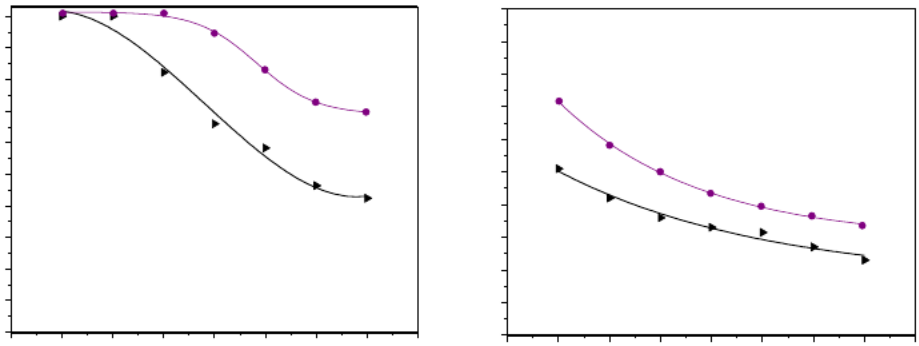

Fig. 13. (A) Glycerol conversion and (B) Acrolein selectivity with time on stream at WHSV = 0.75 h^{-1} and T = 275 °C for the catalysts: ( ) H-ZSM-5 AT NaOH 0.01 mol L^{-1}, ( ) H-AT(0.7).

sion. Table 3 summarized the glycerol conversion, yield to acrolein, and the initial and final selectivities to each compound. Fig. 11 shows the selectivities to the main compounds of this reaction system at different space velocities for the H-AT(0.7) catalyst. It can be observed that as the WHSV increases, the selectivity to acrolein, propanal and acetaldehyde decreases. The amount of acetol remains practically constant; however the quantity of ´others´ is noticeably increased. As above discussed, acrolein is formed by dehydration of glycerol on Brønsted acid sites, whiles acetol is formed on the Lewis acid sites. Results shown in Fig. 11 and Table 3 therefore, imply that the Brønsted acid sites deactivate faster than the Lewis acid sites and for this reason acrolein selectivity decreases with time while acetol selectivity increases. Since the selectivity of the compounds grouped in´others´ increases as the conversion decreases, it is possible to conclude that these compounds are formed directly from the glycerol, being primary products. For this reason, the reaction scheme shown in Fig. 7 includes this reaction step. Fig. S2 (Supplementary Material) shows typical chromatograms at low and high glycerol conversion obtained at 1 h and 7 h on stream respectively. Peaks without labels were not identified, and corresponds to the compounds grouped in 'others'. It can be seen that this group contains several compounds with small area.

The effect of temperature was also studied (Fig. 12). An increase of this variable from 275 °C to 300 °C was detrimental to the catalytic performance of the materials. For example, for the catalyst H-AT(0.7) an important increase in the rate of deactivation was observed, added to a decrease in the selectivity to acrolein. This is associated with the fact that at that temperature the reaction path is favored via acetaldehyde and the formation of coke precursors. In agreement with results shown above, at lower conversion lower acrolein selectivity, what indicates that the Brønsted acid sites involved in the dehydration step deactivates faster than the Lewis sites.

3.9.4. Effect of the anion during the alkaline treatment

Fig. 13 shows the activity results of the H-AT(0.7) catalyst and the results obtained with a H-ZSM-5 zeolite treated with 0.01 mol L^{-1} NaOH solution. It can be seen that in addition to the advantages mentioned above about the material yield in the preparation, the catalytic performance is much better for the zeolite modified with Na_2CO_3. This is attributed to the lower Si/Al ratio of the latter, in which the Si was selectively removed from the zeolite structure.

4. Conclusions

A procedure to develop mesoporosity in an H-ZSM-5 zeolite was studied, consisting in alkaline treatment with Na_2CO_3 aqueous solutions and ionic exchanges with NH_4NO_3 solutions followed by calcinations. The selected concentrations, temperatures and time of treatment were appropriate to reach a selective removal of Si from the zeolite framework, maintaining the Al content, and generating extra mesoporosity. In this manner, the concentration of Brønsted acid sites was improved in the zeolite, and also the accessibility to the active sites. The activity and selectivity was better than in the case of the non-treated zeolite, and furthermore the stability in reaction was increased.

The alkaline treatment with Na_2CO_3 leads to a significantly higher yield during the preparation procedure as compared to the treatment with NaOH. Also the activity results obtained with the material treated with Na_2CO_3 are much better than the observed for the zeolite modified with NaOH at equivalent pH.

The Brønsted acid sites deactivate faster than the Lewis sites, and this behavior leads to a lower acrolein selectivity, and higher selectivity for acetol formation as catalyst deactivates.

Acknowledgements

The authors thank Martina Braun for her technical assistant with measuring the ^{27}Al MAS NMR spectra at the Department of Chemistry and Catalysis Research Center, Technische Universität München, Garching, Germany. The authors wish to acknowledge the financial support received from the following primary funders: Universidad Nacional del Litoral (Santa Fe, Argentina, grant CAID PACT 96), ANPCyT (Argentina) (grant PICT 2013-1252) and CONICET (Argenitna) (grant PIO 13320130100209CO).

References

[1] A. Corma, S. Iborra, A. Velty, Chem. Rev. 107 (2007) 2411–2502.
[2] D.L. Klass, Biomass for Renewable Energy, Fuels, and Chemicals (Chapter 1), Elsevier Inc., Amsterdam, 1998, pp. 1–27.
[3] M. Ayoub, A. Abdullah, Renew. Sust. Energ. Rev. 16 (2012) 2671–2686.
[4] R.L. Maglinao, B.B. He, Ind. Eng. Chem. Res. 50 (2011) 6028–6033.
[5] M. Pagliaro, R. Ciriminna, H. Kimura, M. Rossi, G. Della Pina, Angew. Chem., Int. Ed. 46 (24) (2007) 4434–4440.
[6] C.H. Zhou, J.N. Beltramini, Y.X. Fan, G.O. Lu, Chem. Soc. Rev. 37 (2008) 527–549.
[7] Y. Moro-Oka, W. Ueda, Adv. Catal. 40 (1994) 233–273.
[8] A. Corma, G. Huber, L. Sauvanauda, P. O'Connor, J. Catal. 257 (2008) 163–171.
[9] S.H. Chai, H.P. Wang, Y. Liang, B.Q. Xu, Applied Catal. A: Gen. 353 (2009) 213–222.
[10] J.L. Dubois, C. Duquenne, W. Hölderich, US Patent 7.396.962, 2008.
[11] K. Omata, S. Izumi, T. Murayama, W. Ueda, Catal. Today 201 (2013) 7–11.
[12] S. Ramayya, A. Brittain, C. DeAlmeida, W. Mok, M.J. Antal, Fuel 66 (10) (1987) 1364–1371.
[13] S.H. Chai, H.P. Wang, Y. Liang, B.Q. Xu, Green Chem. 9 (2007) 1130–1136.
[14] L.Z. Tao, S.H. Chai, Y. Zuo, W.T. Zheng, Y. Liang, B.Q. Xu, Catal. Today 158 (2010) 310–316.
[15] J. Deleplanque, J.L. Dubois, J.F. Devaux, W. Ueda, Catal. Today 157 (2010) 351–358.
[16] E. Tsukuda, S. Sato, R. Takahashi, T. Sodesawa, Catal. Commun. 8 (2007) 1349–1353.
[17] A. Alhanash, E.F. Kozhevnikova, I.V. Kozhevnikov, Appl. Catal. A: Gen. 378 (2010) 11–18.
[18] B. Katryniok, S. Paul, M. Capron, C. Lancelot, V. Bellière-Beca, P. Rey, F. Dumeignil, Green Chem. 12 (2010) 1922–1925.
[19] C.J. Jia, Y. Liu, W. Schmidt, A.H. Lu, F. Schüth, J. Catal. 269 (2010) 71–79.
[20] A.S. de Oliveira, S.J.S. Vasconcelos, J.R. de Sousa, F.F. de Sousa, J.M. Filho, A.C. Oliveira, Chem. Eng. J. 168 (2011) 765–774.
[21] H. Atia, U. Armbruster, A. Martin, Appl. Catal. A 393 (2011) 331–339.
[22] C.L. Lima, S.J.S. Vasconcelos, J.M. Filho, B.C. Neto, M.G.C. Rocha, P. Bargiela, A.C. Oliveira, Appl. Catal. A 399 (2011) 50–62.
[23] G. Foo, D. Wei, D. Sholl, C. Sievers, ACS Catal. 4 (2014) 3180–3192.
[24] B. Yilmaz, U. Muller, Top Catal. 52 (2009) 888–895.
[25] E. Taarning, C.M. Osmundsen, X. Yang, B. Voss, S.I. Andersena, C.H. Christensen, Energy Environ. Sci. 4 (2011) 793–804.
[26] K. Egeblad, C.H. Christensen, M. Kustova, Chem. Mater. 20 (2008) 946–960.
[27] J.C. Groen, L.A.A. Peffer, J.A. Moulijn, J. Perez-Ramírez, Colloids Surf. A 241 (2004) 53–58.
[28] B. Vogel, C. Schneider, E. Klemm, Catal. Lett. 79 (2002) 107–112.
[29] S. van Donk, A.H. Janssen, J.H. Bitter, K.P. de Jong, Catal. Rev. 45 (2003) 297.
[30] R. Le Van Mao, S.T. Le, D. Ohayon, F. Caillibot, L. Gelebart, G. Denes, Zeolites 19 (1997) 270.
[31] J. Perez-Ramirez, F. Kapteijn, J.C. Groen, A. Domenech, G. Mul, J.A. Moulijn, J. Catal. 214 (2003) 33.
[32] T. Suzuki, T. Okuhara, Micropor. Mesopor. Mat. 43 (2001) 83.
[33] Y.N. Li, S.L. Liu, Z.K. Zhang, S.J. Xie, X.X. Zhu, L.Y. Xu, Appl. Catal. A 338 (2008) 100.
[34] M. Ogura, S. Shinomiya, J. Tateno, Y. Nara, M. Nomura, E. Kikuchi, M. Matsukata, Appl. Catal. A: General 219 (2001) 33–43.
[35] R. Le Van Mao, S. Xiao, A. Ramsaran, J. Yao, J. Mater. Chem. 4 (1994) 605–610.
[36] J.C. Groen, L.A.A. Peffer, J.A. Moulijn, J. Pérez-Ramírez, Chem. Eur. J. 11 (2005) 4983–4994.
[37] S. Brunauer, P.H. Emmet, E. Teller, J. Am. Chem. Soc. 60 (1938) 309.
[38] B.C. Lippens, J.H. de Boer, J. Catal. 4 (1965) 319.
[39] J.C.P. Broekhoff, J.H. de Boer, J. Catal. 9 (1967) 8.
[40] J. Jiao, J. Kanellopoulos, W. Wang, S. Ray, H. Foerster, D. Freude, M. Hunger, PCCP 7 (2005) 3221–3226.
[41] H. Chen, T. Sun, D. Sui, J. Dong, Anal. Chim. Acta 698 (2011) 27–35.
[42] Y. Gu, N. Cui, Q. Yu, C. Li, Q. Cui, Appl. Catal. A: General 429–430 (2012) 9–16.
[43] H.P. Decolatti, B.O. Dalla Costa, C.A. Querini, Microp. Mesop. Mat. 204 (2015) 180–189.
[44] V. Rac, V. Rakic, Z. Miladinovic, D. Stosic, A. Auroux, Thermochim. Acta 567 (2013) 73–78.
[45] K.S.W. Sing, D.H. Everett, R.A.W. Haul, L. Moscou, R.A. Pierotti, J. Rouquerol, T. Siemieniewska, Pure Appl. Chem. 57 (1985) 603–619.
[46] J.C. Groen, L.A.A. Peffer, J. Pérez-Ramírez, Microporous Mesoporous Mater. 60 (2003) 1–17.
[47] A. Cizmek, B. Subotic, I. Smit, A. Tonejc, R. Aiello, F. Crea, A. Nastro, Microporous Mater. 8 (1997) 159.
[48] C. Su, D.L. Suarez, Clays Clay Miner. 45 (1997) 814–825.
[49] S. Abell, A. Bonilla, J. Perez-Ramirez, Appl. Catal. A 364 (2009) 191–198.
[50] J.C. Groen, J.A. Moulijn, J. Perez-Ramirez, J. Mater. Chem. 16 (2006) 2121–2131.
[51] S.M.T. Almutairi, B. Mezari, G.A. Filonenko, P.C.M.M. Magusin, M.S. Rigutto, E.A. Pidko, E.J.M. Hensen, Chem. Cat. Chem. 5 (2013) 452.
[52] J.P. Marques, I. Gener, P. Ayrault, J.C. Bordado, J.M. Lopes, F. Ramoa Ribeiro, M. Guisnet, Microporous Mesoporous Mater. 60 (2003) 251–262.
[53] C.A. Emeis, J. Catal. 141 (1993) 347–354.
[54] M.R. Nimlos, S.J. Blanksby, X. Qian, M.E. Himmel, D.K. Johnson, J. Phys. Chem. A 110 (2006) 6145.
[55] A. Witsuthammakul, T. Sooknoi, Appl. Catal. A 413–414 (2012) 109–116.
[56] D.M. Bibby, R.F. Howe, G.D. McLellan, Appl. Catal. A 93 (1992) 1–34.
[57] Y.T. Kim, K.D. Jung, E.D. Park, Appl. Catal. A 393 (2011) 275–287.
[58] J. Barrault, J.M. Clacens, Y. Pouilloux, Top. Catal. 27 (2004) 137–142.
[59] A.G. Gayubo, A.T. Aguayo, A. Atutxa, R. Aguado, J. Bilbao, Ind. Eng. Chem. Res. 43 (2004) 2610.
[60] Y.T. Kim, K.D. Jung, E.D. Park, Microporous Mesoporous Mater. 131 (2010) 28–36.